LETTERS
https://doi.org/10.1038/s41477-020-00818-5

nature plants

Check for updates

A transposon surveillance mechanism that safeguards plant male fertility during stress

Yang-Seok Lee[1], Robert Maple[1], Julius Dürr[1], Alexander Dawson[1], Saleh Tamim[2], Charo del Genio[3], Ranjith Papareddy[4], Anding Luo[5], Jonathan C. Lamb[6,10], Stefano Amantia[1], Anne W. Sylvester[5], James A. Birchler[6], Blake C. Meyers[4,7], Michael D. Nodine[8], Jacques Rouster[9] and Jose Gutierrez-Marcos[1]✉

Although plants are able to withstand a range of environmental conditions, spikes in ambient temperature can impact plant fertility causing reductions in seed yield and notable economic losses[1,2]. Therefore, understanding the precise molecular mechanisms that underpin plant fertility under environmental constraints is critical to safeguarding future food production[3]. Here, we identified two Argonaute-like proteins whose activities are required to sustain male fertility in maize plants under high temperatures. We found that MALE-ASSOCIATED ARGONAUTE-1 and -2 associate with temperature-induced phased secondary small RNAs in pre-meiotic anthers and are essential to controlling the activity of retrotransposons in male meiocyte initials. Biochemical and structural analyses revealed how male-associated Argonaute activity and its interaction with retrotransposon RNA targets is modulated through the dynamic phosphorylation of a set of highly conserved, surface-located serine residues. Our results demonstrate that an Argonaute-dependent, RNA-guided surveillance mechanism is critical in plants to sustain male fertility under environmentally constrained conditions, by controlling the mutagenic activity of transposons in male germ cells.

Crop yield loss driven by high temperatures has been widely reported in many species, posing a real threat to food security[2,4]. Plant male reproductive development is especially sensitive to spikes in temperature[5], with direct consequences on fertility and seed productivity[3,6] probably due to metabolic and physiological changes resulting from induced epigenetic perturbations[7]. In rice, the temperature-sensitive genic male sterile mutants *pms3* and *p/tms12-1* have been found to carry mutations in long non-coding RNA precursors that normally produce phased secondary small interfering RNAs[8–10] mainly in developing anthers. The slicing of rice long non-coding RNA phasiRNA (*PHAS*) precursors is directed by two 22-nt micro RNAs (miR2118 and miR2275)[11–13], leading to the formation of double-stranded RNA by RNA-DEPENDENT RNA POLYMERASE-6 (RDR-6)[14], which is sequentially processed by Dicer-like (DCL) proteins DCL4 or DCL5 into 21- or 24-nt phasiRNAs, respectively[15,16]. Interestingly, two rice Argonaute-like (AGO) proteins, AGO 18 and MEIOSIS ARRESTED AT LEPTOTENE-1 (MEL-1), have been found to be associated with 21-nt phasiRNAs and are required for male fertility[12,17,18]. Thus, while the production of phasiRNAs in rice anthers has been linked to male fertility, the precise biological significance of this pathway in plants remains largely unknown.

It has been reported that maize anthers also accumulate two distinct populations of phasiRNAs, which occur at distinct phases of male germ cell development, and that DCL5 is critical for male fertility[19,20]. Of particular interest is the 21-nt phasiRNA subclass, which is abundant in the epidermis of pre-meiotic wild-type anthers but absent in male sterile mutants lacking a functional anther epidermis[19,21]. We postulated that the pre-meiotic phasiRNA pathway might play a critical role in supporting male fertility in plants. To this end, we scanned maize transcriptome data to identify components of the small RNA pathway specifically expressed in the epidermis of pre-meiotic anthers[22]. We identified two Argonaute-like genes with similarity to *Arabidopsis* AGO-5 and rice MEL-1, which we named MALE-ASSOCIATED ARGONAUTE-1 and -2 (MAGO1 and MAGO2) (Supplementary Fig. 1a,b). We found that MAGO1/2 accumulate primarily in the cytoplasm of epidermal cells of pre-meiotic anthers and in the nuclei of developing meiocytes (Supplementary Fig. 1c–e).

To determine the potential roles of MAGO1/2, we first identified transposon insertion mutant alleles for both genes and found that while all wild-type and single-mutant plants grown under field conditions produced fully viable mature pollen, double-mutant plants were male sterile (Supplementary Fig. 2a,b). In addition, we generated *MAGO1/2* RNA interference lines to simultaneously downregulate both genes ($MAGO^{KD}$) (Supplementary Fig. 2c) and found that most $MAGO^{KD}$ lines displayed a range of male sterility phenotypes (non-viable pollen) under field-grown conditions (Fig. 1a and Supplementary Fig. 2d). Taken together, our genetic analyses revealed that MAGO genes act redundantly to support male fertility in maize.

Because the spatial and temporal accumulation of MAGO1/2 mirrors the reported expression of 21-nt phasiRNAs and the predicted miR2118 trigger[19], we next tested whether MAGO1/2 are involved in either the biogenesis or function of these phasiRNAs. We therefore performed immunoprecipitations using specific antisera and sequencing the bound sRNAs. We found that both MAGO1/2

[1]School of Life Sciences, University of Warwick, Coventry, UK. [2]Center for Bioinformatics and Computational Biology, University of Delaware, Newark, DE, USA. [3]Centre for Fluid and Complex Systems, School of Computing, Electronics and Mathematics, Coventry University, Coventry, UK. [4]Division of Plant Sciences, University of Missouri, Columbia, MO, USA. [5]Department of Molecular Biology, University of Wyoming, Laramie, WY, USA. [6]Division of Biological Sciences, University of Missouri, Columbia, MO, USA. [7]Donald Danforth Plant Science Center, St. Louis, MO, USA. [8]Gregor Mendel Institute, Austrian Academy of Sciences, Vienna Biocenter, Vienna, Austria. [9]Biogemma Centre de Recherche de Chappes, Chappes, France. [10]Present address: BayerCrop Science Division, St. Louis, MO, USA. ✉e-mail: J.F.Gutierrez-Marcos@warwick.ac.uk

are associated with pre-meiotic 21-nt phasiRNAs (Supplementary Fig. 3a–d); however, the abundance of these sRNAs was not significantly altered in MAGO^{KD} plants (Supplementary Fig. 3e). This analysis revealed that MAGO1/2 are not directly implicated in the biogenesis of these particular phasiRNAs.

Given that male germline pre-meiotic phasiRNAs in rice are implicated in heat-stress sensitivity and male fertility[9,10], we investigated the effects of heat stress on MAGO1/2 activity in maize. We therefore grew wild-type and MAGO^{KD} plants under controlled-temperature conditions (28/25 °C day/night) and exposed them to a brief heat-stress treatment (35/25 °C day/night) either before or after male meiosis. Under controlled conditions, although we observed slight differences in pollen viability between wild-type and MAGO^{KD} plants these were exacerbated when plants were subjected to heat stress pre-meiotically, with MAGO^{KD} plants becoming largely infertile (Fig. 1b and Supplementary Fig. 4). On the other hand, all plants subjected to heat stress after meiosis showed slightly reduced pollen viability compared with those grown only under controlled conditions, yet no significant difference was observed between wild-type and MAGO^{KD} plants, suggesting that a short exposure to heat stress after meiosis generally affects pollen viability to a lesser extent (Supplementary Fig. 4). Taken together, our genetic analyses revealed that MAGO genes are required before meiosis to support male fertility under heat stress. Furthermore, we postulated that a new class of MAGO-associated, pre-meiotic phasiRNAs might determine male fertility under restrictive temperature conditions. To test this idea, we sequenced sRNAs from pre-meiotic anthers after a short exposure to heat stress. We found that a group of 21-nt phasiRNAs (126/439) were deregulated in MAGO^{KD} plants independently of growth temperature conditions. After heat stress, however, a large fraction of 21-nt phasiRNAs (313/439) accumulated at very high levels in wild-type plants in response to heat stress, but not in MAGO^{KD} plants (Fig. 1c, Supplementary Fig. 5 and Supplementary Table 1). We therefore named this discrete group of sRNAs heat-activated 21-nt phasiRNAs (Hphasi). Analysis of uncapped RNA ends provided strong evidence for miR2118-directed cleavage of Hphasi lncRNA precursors in pre-meiotic wild-type anthers (Supplementary Fig. 6). The spatial distribution of these sRNAs was determined by RNA in situ localization on anther sections from wild-type plants grown under both permissive and restrictive conditions (Fig. 1d). We found that heat stress triggered Hphasi accumulation, primarily in the epidermis of pre-meiotic anthers but also in the inner anther cell layers at the onset of meiosis. However, we did not observe any increase in the accumulation of miR2118 in pre-meiotic anthers after heat stress. We therefore sought to determine whether the biogenesis of these RNAs might play a role in male fertility. Given that helper component-proteinase (HC-Pro) viral silencing suppressor can directly bind and sequester sRNAs[23,24], we reasoned that HC-Pro induction in heat-stressed pre-meiotic anthers could interfere with the biogenesis and/or function of this particular class of phasiRNAs. To test this hypothesis, we first generated transgenic plants carrying a dexamethasone (DEX)-inducible HC-Pro construct. We next immunoprecipitated HC-Pro from DEX-treated anthers and sequenced the bound sRNAs. We found that HC-Pro expression in pre-meiotic anthers was associated with 21-nt phasiRNAs and their predicted miR2188 trigger (Supplementary Fig. 7a–d). To further define the role(s) of these sRNAs, HC-Pro was ectopically expressed in anthers before and after meiosis. Pre-meiotic induction resulted in a near complete lack of pollen grains at anther maturity, whereas post-meiotic HC-Pro induction exerted only minor effects on pollen production (Supplementary Fig. 7e). To establish whether the HC-Pro-mediated effects on male fertility were specifically linked to sRNAs produced in anther epidermal tissues, we generated maize plants with HC-Pro under the control of an epidermal-specific HDZIV6 transactivation system (HDZIV6>>HC-Pro) and confirmed exclusive HC-Pro expression in the anther epidermis by immunolocalization using a specific HC-Pro antibody that we generated (Fig. 1e,f). Notably, we found that the production of pollen grains in HDZIV6>>HC-Pro plants was markedly reduced compared to that in control plants (Fig. 1g). Collectively, these data provide evidence for the activation of a sRNA cascade in anther epidermis that is critical to supporting male fertility under restrictive temperature-stress conditions.

Computational genome-wide scans showed that Hphasi mapped primarily to transposable elements and, specifically, to long terminal repeat retrotransposons (LTRs) within the maize genome (Supplementary Fig. 8a,b). Because transposable elements are typically deregulated in plants during periods of genome shock or abiotic stress[25], we reasoned that Hphasi might be involved in their silencing in anthers following environmental stress exposure. To test this hypothesis, we performed RNA sequencing (RNA-seq) to compare global changes in gene expression in pre-meiotic anthers of MAGO^{KD} and wild-type plants. Under permissive conditions, we did not observe any notable changes in the anther-specific expression of coding genes between wild-type and MAGO^{KD} (Supplementary Fig. 8c). By contrast, exposure to heat stress preceding meiosis resulted in global changes in anther gene expression in all plants tested, independently of genotype (Supplementary Fig. 8c,d and Supplementary Table 2). Notably, we found that LTRs were significantly deregulated in the anthers and meiocytes of MAGO^{KD} plants following heat stress (Fig. 2a,b and Supplementary Table 3). In addition, most of the retrotransposons upregulated in heat-stressed MAGO^{KD} plants were low-copy (<100) retrotransposons of the Gypsy class (LRGs) predicted to be targeted by Hphasi (Supplementary Fig. 9a and Supplementary Table 4). Subsequent analysis of uncapped RNA ends provided strong support for the directed cleavage of LRGs by Hphasi (Fig. 2c and Supplementary Fig. 9b). To test whether MAGO and associated phasiRNAs are involved in modulating the mobility of these LRGs, we carried out transposon display and retrotransposon-sequence capture on progenies generated from reciprocal crosses between wild-type and MAGO^{KD} plants grown under summer field conditions and

Fig. 1 | MAGO and pre-meiotic sRNAs are essential for male fertility in maize. a, Male fertility defects observed in MAGO^{KD} (line T02878_006) and wild-type (WT) plants grown under field conditions. Pollen grains (insets) following Alexander's staining and mature male inflorescences ($n=10$ biological replicates). Scale bar, 5 cm (insets, 200 μm). **b**, Pollen viability in WT and MAGO^{KD} (line T02878_006) plants under controlled permissive conditions (28 °C) and subjected to heat stress (35 °C) before meiosis ($n=10$). Scale bars, 200 μm. **c**, Accumulation of 21-nt phasiRNAs in anthers of WT and MAGO^{KD} (line T02878_006) plants exposed to different temperatures preceding meiosis ($n\geq2$ biologically independent samples each). **d**, In situ RNA localization of Hphasi and miR2118 in anthers of WT plants exposed to heat stress preceding meiosis ($n=2$ biological replicates). Scale bars, 50 μm. Black arrowheads indicate accumulation of sRNAs. **e**, Confocal images of NLS-dTomato reporter expression in anthers of HDZIV>>HC-Pro plants ($n=5$ biological replicates). Scale bars, 50 μm. ep, epidermis; en, endothecium; mid, mid-layer; tp, tapetum; mc, meiocyte. **f**, Immunodetection of HC-Pro in anther epidermis in control and HDZIV>>HC-Pro plants ($n=2$ biological replicates). Scale bars, 50 μm; black arrowhead indicates accumulation of HC-Pro. **g**, Top: pollen viability in anthers from control and HDZIV6>>HC-Pro plants ($n\geq30$) grown under permissive (28 °C) and restrictive (35 °C) temperature conditions. Violin plots show distribution of data, with medians indicated by black boxes and means by asterisks. Differences between groups were determined by one-way analysis of variance (ANOVA), $^{***}P<0.001$. NS, not significant. Bottom: representative anthers following Alexander's staining; scale bars, 100 μm.

which are thus regularly exposed to spikes in temperature. Our analyses revealed retrotransposons to be highly mobile, primarily in the male germ cell lineage of MAGO^{KD} plants (Fig. 2d and Supplementary Table 5).

Our data thus far indicate a role for MAGO proteins in protecting male germ cells from the deregulated activity of retrotransposons that occurs during heat stress. To understand how MAGO activity is regulated by heat stress, we first analysed our RNA-seq data. However, we did not observe significant changes in MAGO transcript levels in response to heat stress (Supplementary Fig. 10), indicating that their activity may be modulated post-translationally. Indeed, previous studies in maize and rice have identified other Argonaute-like

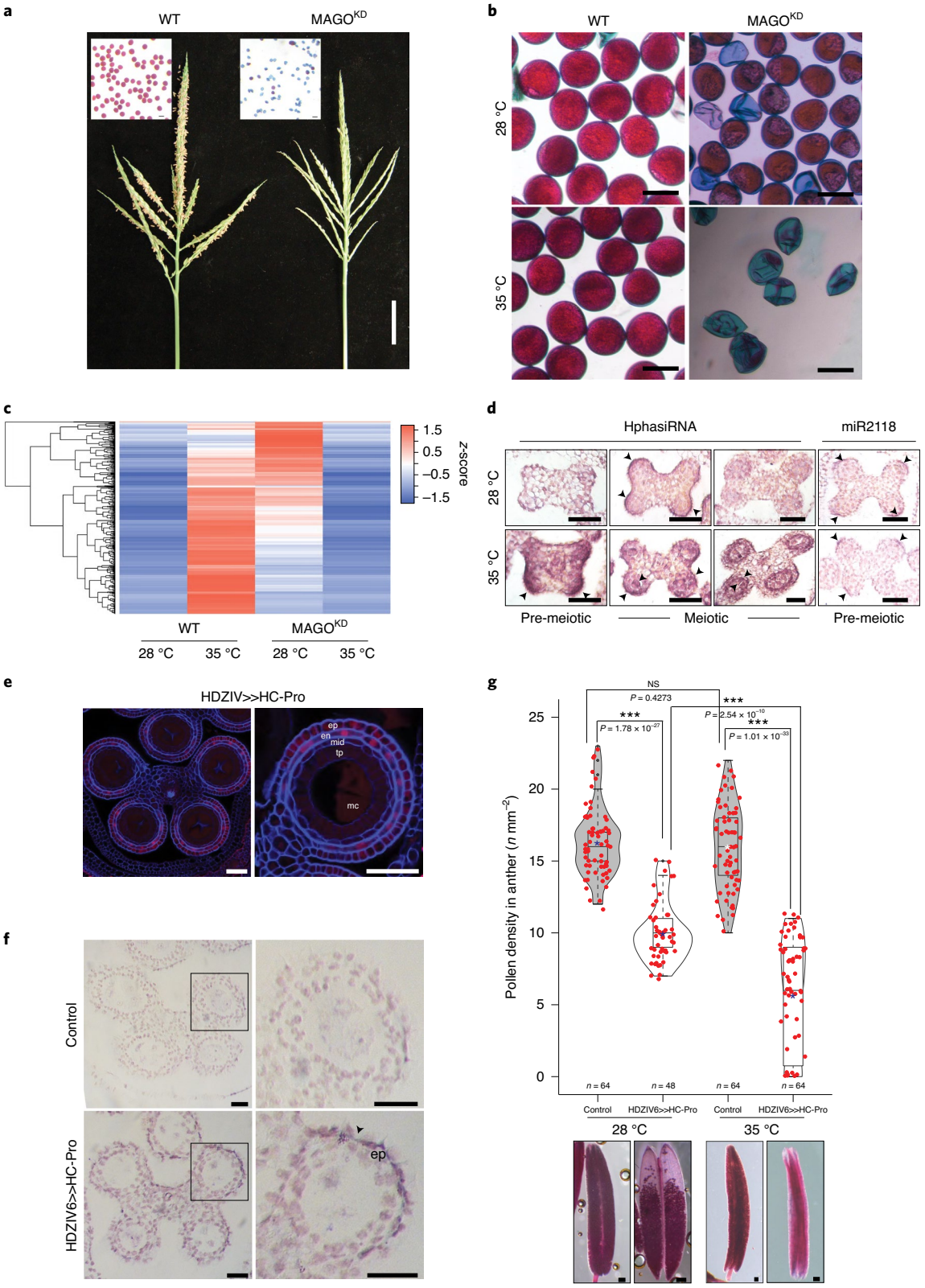

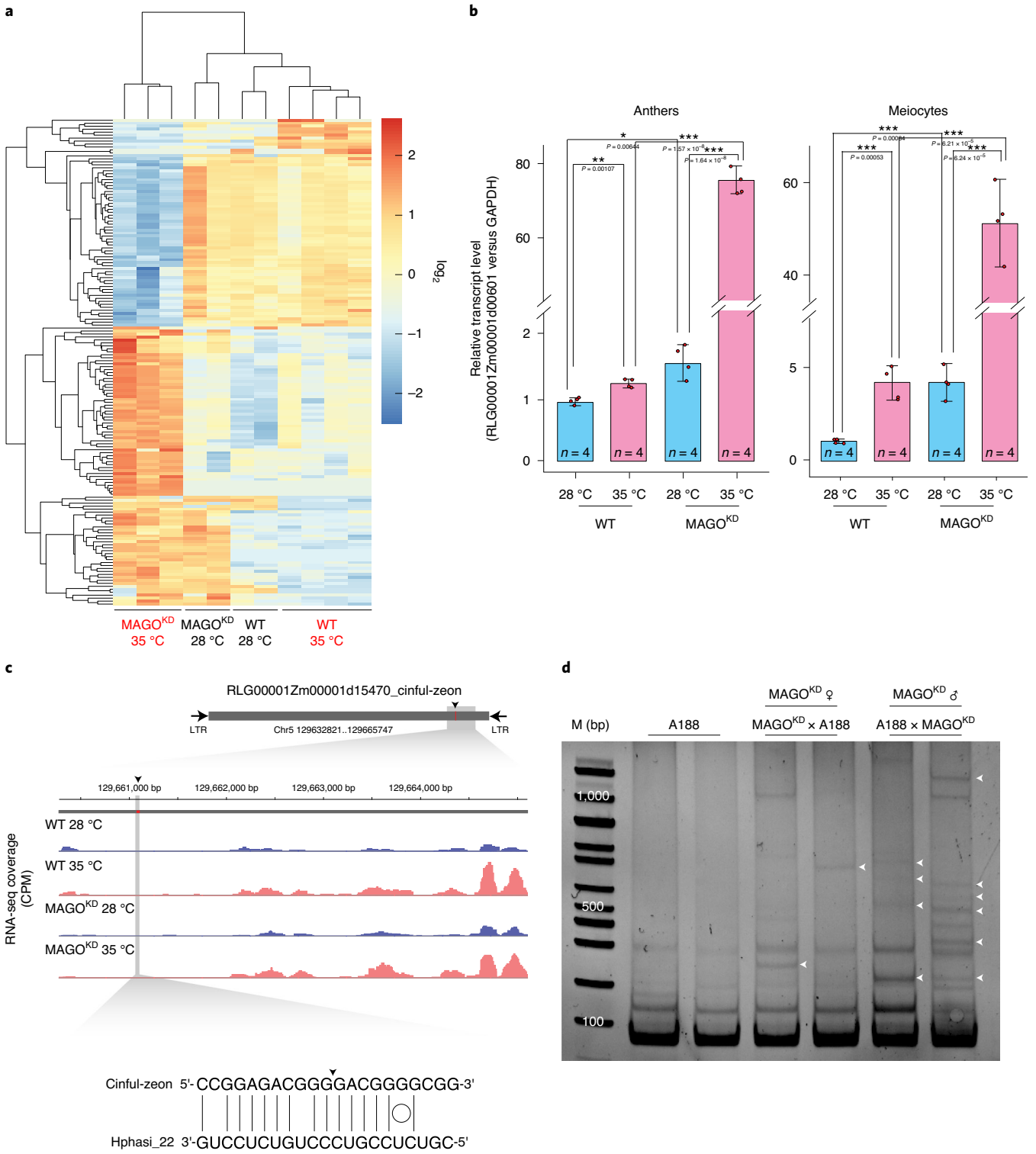

Fig. 2 | MAGO1/2 are necessary to silence stress-activated retrotransposons in maize male germ cells. a, Heatmap analysis of transposon transcripts deregulated in anthers of wild-type (WT) and MAGO^{KD} (line T02878_006) plants exposed to heat stress preceding meiosis ($n \geq 2$ biologically independent samples each). **b**, Relative expression of a MAGO-regulated LTR in anthers and meiocytes of WT and MAGO^{KD} (line T02878_006) plants exposed to heat stress preceding meiosis ($n = 4$ plants). Error bars denote mean values ± s.d. Differences between groups were determined by one-way ANOVA, $^{*}P < 0.05$, $^{**}P < 0.01$, $^{***}P < 0.001$. **c**, Coverage of RNA-seq of retrotransposons targeted by Hphasi in anthers of WT and MAGO^{KD} (line T02878_006) plants exposed to heat stress preceding meiosis ($n \geq 2$ biologically independent samples each). Black arrowhead and red bar, location of predicted sites for Hphasi-directed slicing remnants ($n = 3$ independent samples each); grey box, retrotransposon; black arrows, long terminal inverted repeats. CPM, counts per million reads mapped. **d**, Transposon display showing the presence of retrotransposon insertions in progenies from both WT (A188) plants and reciprocal crosses with MAGO^{KD} (line T02878_006). Each lane represents a pool of 25 independent plants ($n = 2$ biologically independent experiments). White arrowheads indicate new retrotransposon insertions. M, DNA marker; bp, base pair.

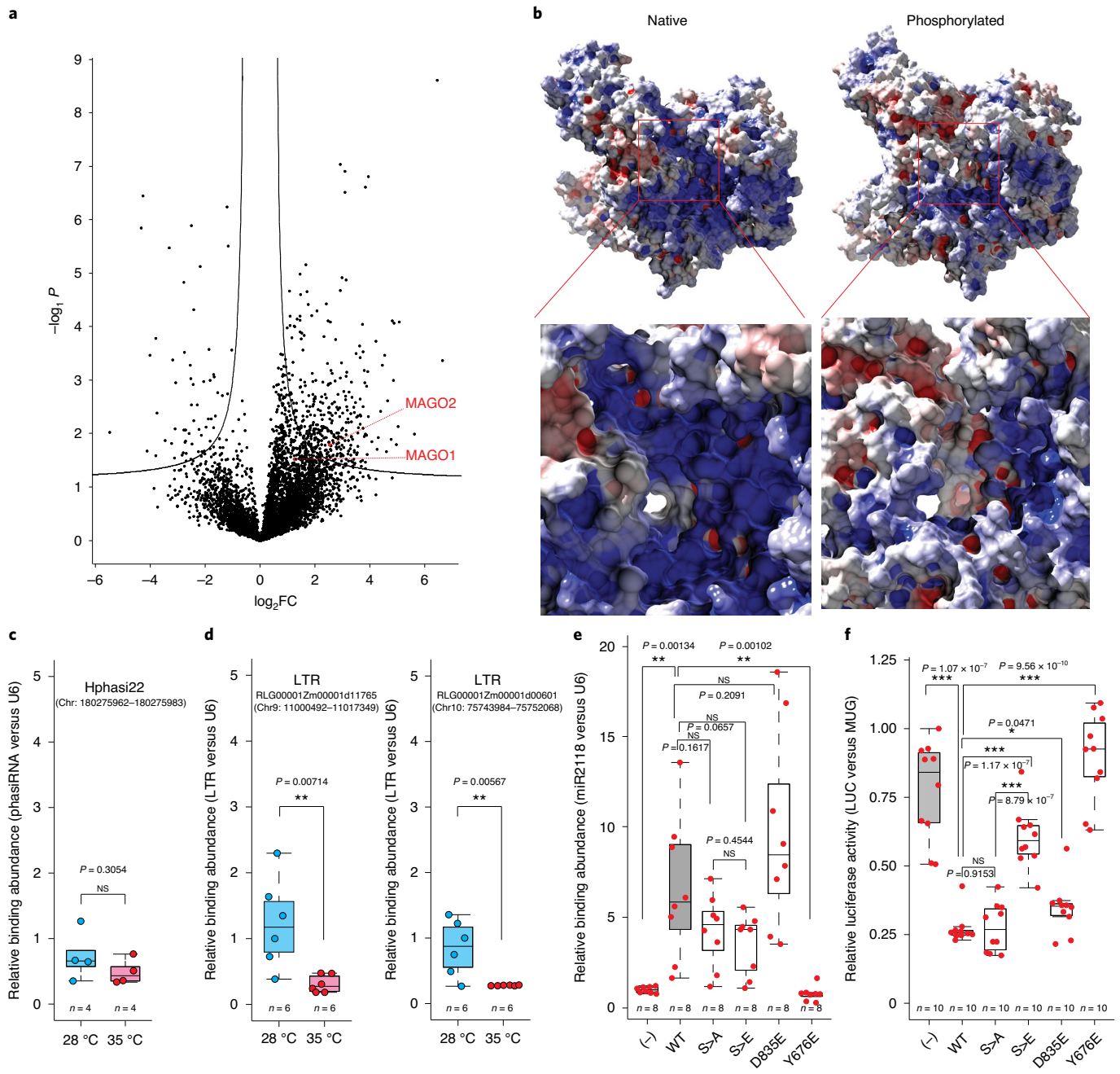

Fig. 3 | MAGO activity is modulated by dynamic changes in phosphorylation induced by heat stress. a, Volcano plot showing dynamic changes in phosphorylation in pre-meiotic anthers after heat stress and identification of differentially phosphorylated MAGO proteins. $\log_2$(fold change) (FC) ratios of the median of biological replicates were plotted versus $-\log_1$ of the *P* values derived from a two-sided Student's *t*-test. The black lines indicate the high significance threshold (FDR < 0.05). MAGO1, $\log_2$FC 1.67, $-\log_1 P$ 1.75; MAGO2, $\log_2$FC 2.30, $-\log_1 P$ 1.87; $n = 6$ independent biological replicates. **b**, Electrostatic potential distribution on the molecular surface of native and phosphorylated MAGO2 showing negative (red), positive (blue) and hydrophobic (grey) residues. Red boxes: close-up views of the central cleft and L2 loop known to be implicated in the regulation of sRNA-target interactions. **c**, Accumulation of Hphasi22 bound to MAGO2, shown by immunoprecipitation coupled to quantitative PCR with reverse transcription (RT–qPCR), in pre-meiotic anthers from wild-type plants exposed to permissive (28 °C) and restrictive (35 °C) temperature conditions; $n = 4$ independent biological replicates. Differences between groups were determined by paired two-sided *t*-test. **d**, Accumulation of retrotransposon RNA bound to MAGO2, shown by immunoprecipitation coupled to RT–qPCR, in pre-meiotic anthers from wild-type plants exposed to control (28 °C) and heat-stress conditions (35 °C); $n = 6$ independent biological replicates. Differences between groups were determined by two-sided *t*-test, $^{**}P < 0.01$. **e**, Abundance of bound sRNAs in wild-type MAGO2 and mutants, shown by immunoprecipitation coupled to RT–qPCR); $n = 10$ independent biological replicates. Differences between groups were determined by one-way ANOVA, $^{**}P < 0.01$. **f**, Silencing activity of MAGO2 in wild-type and MAGO2 mutants for residues implicated in differential phosphorylation (S>A and S>E), and in residues predicted to be necessary for target cleavage (D835E) and sRNA binding (Y676E); $n = 10$ independent biological replicates. Differences between groups were determined by one-way ANOVA, $^{*}P < 0.05$, $^{***}P < 0.001$. **c**–**f**, The boxes span from the first to the third quartiles, the bands inside the boxes represent the medians and the whiskers above and below the boxes represent 1.5× the interquartile range from the quartiles.

proteins that are phosphorylated in anthers[26,27]. We therefore performed phosphoproteome analysis of pre-meiotic wild-type anthers and identified major changes in phosphorylation induced by short exposure to heat stress (Fig. 3a and Supplementary Table 6). Specifically, a region in the PIWI domain of MAGO proteins that contains four serines and one threonine residue was significantly hypophosphorylated in response to heat stress (Supplementary Fig. 11). To further understand the biological significance of these dynamic changes in MAGO phosphorylation, we modelled the structure of the conserved catalytic domain of MAGO2 and analysed the electrostatic potential of the molecular surface of different phosphorylation variants (Fig. 3b and Supplementary Video 1). We found that the residues targeted by phosphorylation are located at the surface of a loop following the PIWI domain (Supplementary Fig. 12). This finding is in line with the conserved presence of phosphorylated serine/threonine residues in the PIWI loops of other catalytically active plant and animal Argonautes (Supplementary Fig. 12b and Supplementary Table 7). These phosphorylated residues are in close proximity to both the central cleft and an L2 loop, which are considered important for the regulation of sRNA–target interactions[28]. Notably, we found that the hyperphosphorylation of S989–S998 does not cause significant changes in MAGO2 structure but is predicted to cause profound changes to the electrostatic surface potential of the upper central cleft region (Fig. 3b). To test whether these stress-induced changes could affect the affinity for sRNAs and/or enzymatic activity of MAGO2, we immunoprecipitated MAGO2 from anthers of plants exposed to a pulse of heat stress preceding meiosis and quantified the bound sRNAs. While we did not find significant differences in the association of MAGO2 with 21-nt Hphasi under control and heat-stress conditions (Fig. 3c), the abundance of retrotransposon RNA targets associated with MAGO2 was significantly reduced after exposure to heat stress (Fig. 3d). Because of this, we reasoned that the changes in surface charge induced by MAGO2 hypophosphorylation could regulate the interaction between sRNA and target to sustain the rapid silencing of deregulated retrotransposons in male germ cells. To test this hypothesis, we generated an in vivo reporter system to test the catalytic activity of wild-type MAGO2 and a series of phosphoresistant (S>A) and phosphomimetic (S>E) MAGO2 mutants (Supplementary Fig. 13). We also generated mutations in MAGO2 residues predicted to be essential for sRNA binding (Y676E) and sRNA-directed RNA cleavage (D835E) for inclusion in this experiment. We found that while sRNA binding was affected in MAGO^{Y676E}, it was not significantly affected in either MAGO$^{S>A}$, MAGO$^{S>E}$ or MAGO^{D835E} (Fig. 3e). Silencing activity was, however, abolished in MAGO^{Y676E} and significantly reduced in only MAGO$^{S>E}$ (Fig. 3f). These data suggest that stress-mediated hypophosphorylation of MAGO2 is important for its effective interaction with retrotransposon RNA targets. This model is consistent with previous studies in humans, which have shown that hyperphosphorylation of the PIWI domain of AGO2 (S824–S834) impairs RNA–target association while hypophosphorylation expands the target repertoire[29,30].

In sum, we have identified in maize two Argonaute-like proteins acting alongside a distinct group of sRNAs in a male-germline-specific manner. This pathway is remarkably similar to the sRNA-mediated recognition pathway found in mammalian male germ cells, which acts to silence retrotransposon activity[31]. Unlike in animals, however, transposon activity is more permissive in plants. For instance, bursts of transposon mobility have helped shape plant genomes and alter transcriptional responses[32]. Furthermore, the insertion of retrotransposons in gene regulatory regions has resulted in marked effects on plant phenotypes—a property that was repeatedly exploited during the process of crop domestication[33]. Nevertheless, plants must regulate retrotransposon activity because, as shown for genomic shock, deregulated retrotransposon activity often results in genomic and epigenomic instability and ultimately causes negative effects on offspring fitness[25]. Our findings reveal an Argonaute-mediated pathway that protects plant male fertility by acting as a pre-meiotic surveillance mechanism activated in the somatic cells surrounding germ cell precursors. The biological significance of this molecular pathway operating under heat-stress conditions to restrict retrotransposon activity in developing male germ cells may be in prevention of the widespread transmission of unwanted or deleterious mutations in wind-pollinated plants such as grasses[34–36]. The manipulation of this molecular mechanism in crops will undoubtedly become a useful strategy in future efforts to enhance male fertility and sustain seed productivity under unpredictable and stressful climatic conditions.

Methods

Plant material and growth conditions. The maize cultivar A188 was used in all experiments. Plants were grown at 28/25 °C day/night in a 16/8 h light/dark cycle under light intensity of 230 μE m^{-2} s^{-1}. Seeds were germinated in pots (diameter 7.62 cm) containing peat-based soil, and grown for 3 weeks before transfer to 28-cm or 40-l pots to flowering. Plants grown under summer field conditions (Iowa, USA) were exposed to day/night-time temperature ranges of 25–40/20–25 °C. Anthers were manually dissected at the V12 stage, and meiotic stage was determined by acetocarmine staining. For heat-stress experiments under controlled environment conditions, maize plants grown in 28-cm pots were transferred to growth chambers for 3 d (16 h light at 35 °C/8 h dark at 25 °C, light intensity 230 μE m^{-2} s^{-1}, humidity 75%). Tobacco plants (*Nicotiana benthamiana*) were grown on M2 soil (Levington Advance) at 22 °C in a 16/8-h light/dark cycle under light intensity of 100 μE m^{-2} s^{-1}.

Identification of transposon insertion mutants. To identify transposon insertion lines for Zm00001d007786 (GRMZM2G05903) and Zm00001d013063 (GRMZM2G123063), we screened a Mutator insertion mutant population generated by Biogemma, an Ac/Ds mutant population[37] and a UniformMu mutant population[38]. Insertion lines were confirmed by PCR (Supplementary Table 6) and back-crossed to A188 inbred for four generations before analysis.

Vector construction and generation of transgenic plants. We generated a MAGO1/2-RNAi vector by subcloning a portion corresponding to positions 2151–2400 of Zm00001d007786 (GRMZM2G05903) and a fragment corresponding to positions 1001–1250 of Zm00001d013063 (GRMZM2G123063) into a pCsVMV::intOsActin-intStLS1-terSbHSP vector using Golden Gate cloning.

To generate a chemically inducible HC-Pro construct, we synthetized a 2,211-base pair (bp) fragment from the wheat streak mosaic virus containing Gateway Recombination flanking sequences (Invitrogen). The synthetic fragment was subcloned into a two-component, DEX-inducible expression binary vector named pZZ-TOP, which is derived from pTF101.1 and carries a LhG4:GR synthetic gene fusion and a bidirectional pOp6 promoter[39]. This vector enables the co-expression of a β-glucuronidase (GUS) reporter and HC-Pro after exposure to 20 mM DEX.

To enable the epidermal expression of HC-Pro, we generated a pZmHDZIV6-LhG4 vector using MultiSite Gateway Recombination (Invitrogen). The native 3,164-bp promoter and the 945-bp native terminator of Zm00001d002234 (GRMZM2G001289) were cloned into pDONR221 P1–P4 and pDONR221 P3–P2, respectively. The maize codon-optimized LhG4 was cloned into pDONR221 P4r–P3r. The resulting three entry vectors were then recombined into the binary vector pAL010, a derivative of pTF101.1 carrying a Gateway Recombination Cassette and a bidirectional pOp6 promoter enabling the co-expression of GUS and NLS-tdTomato reporters. All constructs were fully sequenced before transformation in maize using *Agrobacterium tumefaciens* strain LBA4404 (MAGO1/2-RNAi and pZmHDZIV6-LhG4) or EHA101 (HC-Pro).

To determine the in vivo activity of MAGO proteins, we generated a firefly luciferase silencing reporter system. First, we generated a construct containing a nopaline synthase (NOS) promoter (pNOS), a firefly luciferase fused to four miR2118 target sequences, a truncated green fluorescent protein (ΔGFP) and a NOS terminator (tNOS). This synthetic fragment was cloned in pBINPLUS using *Hin*dIII and *Bam*HI restriction enzyme digestion. The miR2118 target region was designed to have optimal hybridization energies with the RNA target. The resulting construct was digested with *Sma*I and *Eco*RI to enable the insertion of a p35S::GUS:tNOS fragment derived from the pSLJ4J8 vector. We also generated a fragment containing the octopine synthase promoter, an artificial miRNA based on maize miR2118c (amiR2118) and a NOS terminator. This fragment was cloned into pBINPLUS using *Asc*I restriction enzyme digestion. To simultaneously express MAGO and amiR2118, we generated codon-optimized MAGO1 and 2 containing a FLAG tag at the carboxy-terminal end, which were cloned into pCsVMV::intOsActin-terSbHSP using SapI, resulting in the binary vectors pBIOS11743 and pBIOS11746, respectively. For the phosphorylation study, we generated codon-optimized MAGO2 phosphomimetic (S>E) and phosphoresistant

(S>A) forms containing a FLAG tag at the carboxy end, which were cloned into pCsVMV::intOsActin-terSbHSP using SapI, resulting in the binary vectors pBIOS11747 and pBIOS11748, respectively. MAGO2 mutants for sRNA binding (Y676E) and cleavage (D835E) were generated using a Q5 Site-Directed Mutagenesis Kit (NEB). Next, pOCS::amiR2118:tNOS was subcloned into pBIOS11743 and pBIOS11746 using AscI restriction enzyme digestion. Generated constructs were fully sequenced and transformed in *N. benthamiana* using *A. tumefaciens* GV3101.

To study in vivo localization of MAGO proteins, codon-optimized coding regions for each gene were subcloned in pGWB441 (ref. [40]) to generate C-terminal EYFP protein fusion after Gateway Recombination (Invitrogen). All constructs generated in this study were fully sequenced and transformed in *N. benthamiana* using *A. tumefaciens* GV3101.

Antiserum preparation and immunopurification. Polyclonal antisera were raised in rabbit against synthetic peptides for MAGO1 (VETEHQQGKRSIYRI) or MAGO2 (CVAAREGPVEVRQLPK) (Eurogentec). To generate HC-Pro antisera, a partial DNA fragment was chemically synthesized (Integrated DNA Technology) and cloned in pET29a (Novagen, Merck). A soluble fraction of HC-Pro was isolated and purified by metal affinity chromatography and polyclonal antiserum was raised in rabbit (Eurogentec). All antisera were affinity purified using a Sulpholink coupling gel system (Pierce).

Sequencing data and statistics analyses. Analyses of sRNA sequencing data were carried out using previously described methods[41]. Sequences obtained from sRNA-seq were processed to remove adaptors and low-quality reads, with lengths of 15–34 nt. After exclusion of those matching structural RNAs (transfer RNA or ribosomal RNA loci), sRNA reads were mapped perfectly (with no mismatches) back to the maize B73 reference genome AGPv4 with Shortstack using Bowtie2 (ref. [42]). Any read with >50 perfect matches (hits) to the genome was excluded from further analysis. Abundances of sRNAs in each library were normalized to transcripts per 10 million, based on the total count of genome-matched reads in that library and the differential sRNA expression determined ($\log_2$FC > 1, $P < 0.001$) using DEseq2 (ref. [43]). For the analysis of RNA-seq data, reads were trimmed and mapped to maize B73 reference genome AGPv4 using TopHat2 (ref. [44]), and differential expression of annotated genes and transposons ($\log_2$FC > 1; $P < 0.001$) was quantified using TEtranscripts[45]. For the NanoPARE sequencing data analysis (software code available at GitHub; https://github.com/Gregor-Mendel-Institute/NanoPARE), we used a defined analysis pipeline and EndCut to determine candidates for sRNA-mediated cleavage of retrotransposons[46]. FASTQ files were mapped to the AGPv4 reference genome and sequences were trimmed using Cutadapt[47]. Reads showing low sequence complexity ($I < 0.15$, where I is the low sequence complexity index) were eliminated and the remaining reads were realigned using STAR[48]. To detect sRNA-mediated cleavage sites, miRNA and phasiRNA sequences were selected and randomized 1,000× each. Target sites were defined based on the level of complementarity between sRNAs and transcripts computed using Allen scores derived from the position and frequency of the miRNA–target duplex mismatches[49]. For the predicted target sites we used the EndGraph output with EndCut_step1.sh, thus allowing the quantification of reads at target sites and within 20/50-nt regions. Neighbouring sites within 1 nt of the predicted cleavage sites were not considered so as not to penalize sites for sRNA isoforms with small offset target recognition sites. We calculated local enrichment of NanoPARE read 5′-ends at cleavage sites by dividing nanoPARE read 5′ ends at cleavage +1 by the numbers of reads in adjacent transcript regions +1. Each of the predicted cleavage sites detected was also assigned an Allen score, and EndCut_step2.R was used to compute empirical aggregate distribution functions of fold changes (ECDFFC) and Allen scores (ECDFAS) for each randomized sRNA control set. These served as null models to assess whether the cleavage site fold changes observed differed from ECDFFC, and whether the observed site Allen scores were larger than ECDFAS. The final P values for each site were calculated by combining Fisher's test P values with probability testing, and adjusted for multiple testing employing Benjamini–Hochberg correction. We defined as significant cleavage sites only those with $P < 0.05$, FC > 1.0 and >1.0 reads per 10 million transcriptome-mapping reads.

Phosphoproteomic analysis. Protein from anthers was extracted by adding three times the volume of extraction buffer (50 mM HEPES, 150 mM NaCl, 1 mM EDTA, 20 mM NaF, 1 mM Na_2MoO_4, 1% (v/v) SDS, 1 mM phenylmethyl sulfonyl fluoride, 2 µM Calyculin A, 1 mM $NaVO_4$, 1 mM DTT and Protease inhibitor cocktail (Roche)) to 0.5 g of tissue. After 30 min the samples were spun for 15 min at 4,000*g* (4 °C) to remove debris. The supernatant was transferred to a new tube, centrifuged for 30 min at 16,000*g* (4 °C), transferred to a new tube and treated using the FASP protocol[50]. Samples were loaded on Amicon Ultra 2-ml Centrifugal Filters with a cut-off of 3 kDa and diluted with 1 ml of 8 M urea until 1 ml of buffer had passed through the column. Reduction and alkylation of cysteine residues was carried out by adding a combination of 5 mM Tris (2-carboxyethyl) phosphine and 10 mM iodoacetamide for 30 min at room temperature in the dark, followed by six washes with 25 mM Hepes pH 7.5. Protein was digested with trypsin (Promega Trypsin Gold, mass spectrometry grade) overnight at 37 °C at an enzyme:substrate ratio of 1:100 (w:w). After digestion, peptides were suspended in 80% acetonitrile (AcN) and 5% trifluoroacetic acid (TFA), and insoluble matter was spun down at 4,000*g* for 10 min. The supernatant was used for the enrichment of phosphopeptides as previously described, with minor modifications[51]. Peptide concentration was measured with a Qubit fluorometer (Invitrogen) and 1 µg of total peptides used for each sample. Titansphere TiO_2 10-µm beads (GL Sciences) were equilibrated in a buffer containing 20 mg ml^{-1} 2,5-dihydroxybenzoic acid (DHB), 80% AcN and 5% TFA in 10 µl of DHBeq per 1 mg beads for 10 min with gentle shaking at 600 r.p.m. TiO_2 beads were used in a peptide:beads ratio of 1:2 (w:w). TiO_2 solution was added to each sample and incubated for 60 min at room temperature; this step was repeated once. The samples were then spun down at 3,000*g* for 2 min and resuspended in 100 µl of Wash buffer I (10% AcN, 5% TFA). The resuspended beads were added to self-made C8 columns comprising 200-µl pipette tips with 2-mm Empore Octyl C8 (Supelco) discs. The columns were spun down at 2,600*g* for 2 min and washed with 100 µl of Wash buffer II (40% AcN, 5% TFA) and 100 µl of Wash buffer III (40% AcN, 5% TFA). Peptides were eluted from the TiO_2 beads with 20 µl of 5% ammonium hydroxide and subsequently with 20 µl of 20% ammonium hydroxide in 25% AcN. Both eluates were pooled, the volume was reduced to 5 µl in a centrifugal evaporator (20–30 min) followed by acidification with 100 µl of buffer A (2% AcN, 1% TFA). Samples were desalted with a self-made C18 column (Empore Octadecyl C18). C18 columns were created in the same way as the C8 columns. Before addition of samples, the C18 columns were activated with 50 µl of methanol and washed with 50 µl each of AcN and buffer A* (2% AcN, 0.1% TFA). Samples were loaded on the C18 column and spun at 2,000*g* for 7 min. The columns were washed with 50 µl each of ethyl acetate and buffer A* and then eluted consecutively with 20 µl each of 40% AcN and 60% AcN. Samples were then vacuum-dried and, before mass spectrometry (MS) analysis, resuspended in 50 µl of buffer A*.

Mass spectrometry data analysis. Label-free peptide relative quantification analysis was performed in Progenesis QI for Proteomics (Nonlinear Dynamics). To identify peptides, peak lists were created using Progenesis QI. The raw data were searched against the maize B73 RefGen_4 Working Gene set. Peptides were generated from tryptic digestion with up to two missed cleavages, carbamidomethylation of cysteines as fixed modifications and oxidation of methionine and phosphorylation of serine, threonine and tyrosine as variable modifications. Precursor mass tolerance was 5 ppm and product ions were searched at 0.8-Da tolerance. Scaffold (TM, v.4.4.5, Proteome Software) was used to validate tandem MS (MS/MS)-based peptide and protein identification. Peptide identifications were accepted if they could be established at >95.0% probability by the Scaffold Local false discovery rate (FDR) algorithm. Protein identifications were accepted if they could be established at >99.0% probability and contained at least one identified peptide. Proteins containing similar peptides and that could not be differentiated based on MS/MS analysis alone were grouped to satisfy the principles of parsimony. Student's t-test for binary comparisons was used to identify proteins considered differentially phosphorylated between plants treated at 28 and 35 °C with $-\log_1 P > 1.0$ and >1.5-fold change in abundance. We set FDR < 0.05 to identify proteins with the highest level of significance. Differentially accumulated phosphopeptides are listed in Table 4.

Reporting Summary. Further information on research design is available in the Nature Research Reporting Summary linked to this article.

Data availability

Sequence data (messenger RNA-seq, nanoPARE-seq, sRNA-seq and LTR-seq) that support the findings of this study have been deposited at the European Nucleotide Archive under accession code ERP118841. Mass spectrometry proteomics data have been deposited at the ProteomeXchange Consortium with the dataset identifier PXD013891.

Received: 8 April 2020; Accepted: 5 November 2020;
Published online: 4 January 2021

References

1. Challinor, A. J. et al. A meta-analysis of crop yield under climate change and adaptation. *Nat. Clim. Change* **4**, 287–291 (2014).
2. Peng, S. et al. Rice yields decline with higher night temperature from global warming. *Proc. Natl Acad. Sci. USA* **101**, 9971–9975 (2004).
3. Hedhly, A., Hormaza, J. I. & Herrero, M. Global warming and sexual plant reproduction. *Trends Plant Sci.* **14**, 30–36 (2009).
4. Lobell, D. B. & Asner, G. P. Climate and management contributions to recent trends in U.S. agricultural yields. *Science* **299**, 1032 (2003).
5. De Storme, N. & Geelen, D. The impact of environmental stress on male reproductive development in plants: biological processes and molecular mechanisms. *Plant Cell Environ.* **37**, 1–18 (2014).
6. Barnabas, B., Jager, K. & Feher, A. The effect of drought and heat stress on reproductive processes in cereals. *Plant Cell Environ.* **31**, 11–38 (2008).

7. Begcy, K. & Dresselhaus, T. Epigenetic responses to abiotic stresses during reproductive development in cereals. *Plant Reprod.* **31**, 343–355 (2018).
8. Ding, J. et al. A long noncoding RNA regulates photoperiod-sensitive male sterility, an essential component of hybrid rice. *Proc. Natl Acad. Sci. USA* **109**, 2654–2659 (2012).
9. Fan, Y. et al. PMS1T, producing phased small-interfering RNAs, regulates photoperiod-sensitive male sterility in rice. *Proc. Natl Acad. Sci. USA* **113**, 15144–15149 (2016).
10. Zhou, H. et al. Photoperiod- and thermo-sensitive genic male sterility in rice are caused by a point mutation in a novel noncoding RNA that produces a small RNA. *Cell Res.* **22**, 649–660 (2012).
11. Johnson, C. et al. Clusters and superclusters of phased small RNAs in the developing inflorescence of rice. *Genome Res.* **19**, 1429–1440 (2009).
12. Komiya, R. et al. Rice germline-specific Argonaute MEL1 protein binds to phasiRNAs generated from more than 700 lincRNAs. *Plant J.* **78**, 385–397 (2014).
13. Araki, S. et al. miR2118-dependent U-rich phasiRNA production in rice anther wall development. *Nat. Commun.* **11**, 3115 (2020).
14. Song, X. et al. Rice RNA-dependent RNA polymerase 6 acts in small RNA biogenesis and spikelet development. *Plant J.* **71**, 378–389 (2012).
15. Song, X. et al. Roles of DCL4 and DCL3b in rice phased small RNA biogenesis. *Plant J.* **69**, 462–474 (2012).
16. Xia, R. et al. 24-nt reproductive phasiRNAs are broadly present in angiosperms. *Nat. Commun.* **10**, 627 (2019).
17. Das, S., Swetha, C., Pachamuthu, K., Nair, A. & Shivaprasad, P. V. Loss of function of *Oryza sativa* Argonaute 18 induces male sterility and reduction in phased small RNAs. *Plant Reprod.* **33**, 59–73 (2020).
18. Nonomura, K. et al. A germ cell-specific gene of the ARGONAUTE family is essential for the progression of premeiotic mitosis and meiosis during sporogenesis in rice. *Plant Cell* **19**, 2583–2594 (2007).
19. Zhai, J. et al. Spatiotemporally dynamic, cell-type-dependent premeiotic and meiotic phasiRNAs in maize anthers. *Proc. Natl Acad. Sci. USA* **112**, 3146–3151 (2015).
20. Teng, C. et al. Dicer-like 5 deficiency confers temperature-sensitive male sterility in maize. *Nat. Commun.* **11**, 2912 (2020).
21. Vernoud, V. et al. The HD-ZIP IV transcription factor OCL4 is necessary for trichome patterning and anther development in maize. *Plant J.* **59**, 883–894 (2009).
22. Dukowic-Schulze, S. et al. The transcriptome landscape of early maize meiosis. *BMC Plant Biol.* **14**, 118 (2014).
23. Shiboleth, Y. M. et al. The conserved FRNK box in HC-Pro, a plant viral suppressor of gene silencing, is required for small RNA binding and mediates symptom development. *J. Virol.* **81**, 13135–13148 (2007).
24. Lakatos, L. et al. Small RNA binding is a common strategy to suppress RNA silencing by several viral suppressors. *EMBO J.* **25**, 2768–2780 (2006).
25. Lisch, D. How important are transposons for plant evolution? *Nat. Rev. Genet.* **14**, 49–61 (2013).
26. Ye, J. et al. Proteomic and phosphoproteomic analyses reveal extensive phosphorylation of regulatory proteins in developing rice anthers. *Plant J.* **84**, 527–544 (2015).
27. Walley, J. W. et al. Integration of omic networks in a developmental atlas of maize. *Science* **353**, 814–818 (2016).
28. Sheu-Gruttadauria, J., Xiao, Y., Gebert, L. F. & MacRae, I. J. Beyond the seed: structural basis for supplementary microRNA targeting by human Argonaute2. *EMBO J.* **38**, e101153 (2019).
29. Quevillon Huberdeau, M. et al. Phosphorylation of Argonaute proteins affects mRNA binding and is essential for microRNA-guided gene silencing in vivo. *EMBO J.* **36**, 2088–2106 (2017).
30. Golden, R. J. et al. An Argonaute phosphorylation cycle promotes microRNA-mediated silencing. *Nature* **542**, 197–202 (2017).
31. Ernst, C., Odom, D. T. & Kutter, C. The emergence of piRNAs against transposon invasion to preserve mammalian genome integrity. *Nat. Commun.* **8**, 1411 (2017).
32. Naito, K. et al. Unexpected consequences of a sudden and massive transposon amplification on rice gene expression. *Nature* **461**, 1130–1134 (2009).
33. Studer, A., Zhao, Q., Ross-Ibarra, J. & Doebley, J. Identification of a functional transposon insertion in the maize domestication gene tb1. *Nat. Genet.* **43**, 1160–1163 (2011).
34. Carpentier, M. C. et al. Retrotranspositional landscape of Asian rice revealed by 3000 genomes. *Nat. Commun.* **10**, 24 (2019).
35. Dooner, H. K. et al. Spontaneous mutations in maize pollen are frequent in some lines and arise mainly from retrotranspositions and deletions. *Proc. Natl Acad. Sci. USA* **116**, 10734–10743 (2019).
36. Peng, Y. et al. Elimination of a retrotransposon for quenching genome instability in modern rice. *Mol. Plant* **12**, 1395–1407 (2019).
37. Li, Y., Segal, G., Wang, Q. & Dooner, H. K. Gene tagging with engineered Ds elements in maize. *Methods Mol. Biol.* **1057**, 83–99 (2013).
38. McCarty, D. R. et al. Steady-state transposon mutagenesis in inbred maize. *Plant J.* **44**, 52–61 (2005).
39. Samalova, M., Brzobohaty, B. & Moore, I. pOp6/LhGR: a stringently regulated and highly responsive dexamethasone-inducible gene expression system for tobacco. *Plant J.* **41**, 919–935 (2005).
40. Nakagawa, T. et al. Improved gateway binary vectors: high-performance vectors for creation of fusion constructs in transgenic analysis of plants. *Biosci. Biotechnol. Biochem.* https://doi.org/10.1271/bbb.70216 (2007).
41. Zhai, J. et al. Spatiotemporally dynamic, cell-type-dependent premeiotic and meiotic phasiRNAs in maize anthers. *Proc. Natl Acad. Sci. USA* https://doi.org/10.1073/pnas.1418918112 (2015).
42. Langmead, B. & Salzberg, S. L. Fast gapped-read alignment with Bowtie 2. *Nat. Methods* **9**, 357–359 (2012).
43. Love, M. I., Huber, W. & Anders, S. Moderated estimation of fold change and dispersion for RNA-seq data with DESeq2. *Genome Biol.* **15**, 550 (2014).
44. Kim, D. et al. TopHat2: accurate alignment of transcriptomes in the presence of insertions, deletions and gene fusions. *Genome Biol.* https://doi.org/10.1186/gb-2013-14-4-r36 (2013).
45. Jin, Y., Tam, O. H., Paniagua, E. & Hammell, M. TEtranscripts: a package for including transposable elements in differential expression analysis of RNA-seq datasets. *Bioinformatics* https://doi.org/10.1093/bioinformatics/btv422 (2015).
46. Schon, M. A., Kellner, M. J., Plotnikova, A., Hofmann, F. & Nodine, M. D. NanoPARE: parallel analysis of RNA 5′ ends from low-input RNA. *Genome Res.* https://doi.org/10.1101/gr.239202.118 (2018).
47. MARTIN, M. Cutadapt removes adapter sequences from high-throughput sequencing reads. *EMBnet J.* **17**, 10–12 (2011).
48. Dobin, A. et al. STAR: ultrafast universal RNA-seq aligner. *Bioinformatics* **29**, 15–21 (2013).
49. Allen, E. et al. Evolution of microRNA genes by inverted duplication of target gene sequences in *Arabidopsis thaliana*. *Nat. Genet.* **36**, 1282–1290 (2004).
50. Wiśniewski, J. R., Zougman, A., Nagaraj, N. & Mann, M. Universal sample preparation method for proteome analysis. *Nat. Methods* https://doi.org/10.1038/nmeth.1322 (2009).
51. Thingholm, T. E., Jørgensen, T. J. D., Jensen, O. N. & Larsen, M. R. Highly selective enrichment of phosphorylated peptides using titanium dioxide. *Nat. Protoc.* https://doi.org/10.1038/nprot.2006.185 (2006).

Acknowledgements

We thank G. Grant and P. Watson for help with plant husbandry, L. M. Costa for discussions and comments on the manuscript and N. Springer and S. Anderson for help with transposon analysis. This research was supported by awards from the US National Science Foundation (nos. 1027445 to A.W.S. and 1649424 and 1754097 to B.C.M.), European Research Council (grant no. 637888 to M.D.N.) and Biotechnology and Biological Sciences Research Council (BBSRC) (nos. BB/L003023/1, BB/N005279/1, BB/N00194X/1 and BB/P02601X/1 to J.G.-M).

Author contributions

Y.-S.L. and R.M. cultivated plants, harvested samples and collected phenotypic data. R.P., J.G.-M. and J.R. identified transposon insertions. J.D. performed phosphoproteome analysis. R.M. and Y.-S.L. performed immunoprecipitation and sRNA-seq libraries. A.L. and J.C.L. generated constructs and transgenic lines for HC-Pro and HDZIV6 transactivation. R.P. constructed nanoPARE libraries. R.M., A.D., S.T., S.A. and M.D.N. performed bioinformatic analysis. C.d.G. performed molecular dynamics simulation and protein modelling. Y.-S.L., R.M., J.D., A.D., S.T. and C.d.G. prepared figures and tables. A.W.S., J.B., B.C.M., M.D.N., J.R. and J.G.-M. co-ordinated experiments. Y.-S.L., R.M. and J.G.-M. conceived the project. J.G.-M. wrote the manuscript with input from the rest of the authors.

Competing interests

The authors declare no competing interests.

Additional information

Supplementary information is available for this paper at https://doi.org/10.1038/s41477-020-00818-5.

Correspondence and requests for materials should be addressed to J.G.-M.

Peer review information *Nature Plants* thanks the anonymous reviewers for their contribution to the peer review of this work.

Reprints and permissions information is available at www.nature.com/reprints.

Publisher's note Springer Nature remains neutral with regard to jurisdictional claims in published maps and institutional affiliations.

nature research

Corresponding author(s): Prof. Jose Gutierrez-Marcos

Last updated by author(s): 21/10/2020

Reporting Summary

Nature Research wishes to improve the reproducibility of the work that we publish. This form provides structure for consistency and transparency in reporting. For further information on Nature Research policies, see our Editorial Policies and the Editorial Policy Checklist.

Statistics

For all statistical analyses, confirm that the following items are present in the figure legend, table legend, main text, or Methods section.

n/a	Confirmed	
☐	☒	The exact sample size (*n*) for each experimental group/condition, given as a discrete number and unit of measurement
☐	☒	A statement on whether measurements were taken from distinct samples or whether the same sample was measured repeatedly
☐	☒	The statistical test(s) used AND whether they are one- or two-sided *Only common tests should be described solely by name; describe more complex techniques in the Methods section.*
☐	☒	A description of all covariates tested
☒	☐	A description of any assumptions or corrections, such as tests of normality and adjustment for multiple comparisons
☐	☒	A full description of the statistical parameters including central tendency (e.g. means) or other basic estimates (e.g. regression coefficient) AND variation (e.g. standard deviation) or associated estimates of uncertainty (e.g. confidence intervals)
☐	☒	For null hypothesis testing, the test statistic (e.g. *F*, *t*, *r*) with confidence intervals, effect sizes, degrees of freedom and *P* value noted *Give P values as exact values whenever suitable.*
☒	☐	For Bayesian analysis, information on the choice of priors and Markov chain Monte Carlo settings
☒	☐	For hierarchical and complex designs, identification of the appropriate level for tests and full reporting of outcomes
☒	☐	Estimates of effect sizes (e.g. Cohen's *d*, Pearson's *r*), indicating how they were calculated

Our web collection on statistics for biologists contains articles on many of the points above.

Software and code

Policy information about availability of computer code

Data collection	All data was collected using standard software. Information is provided in methods section.
Data analysis	All the data was analyzed using publicly available source code and parameters have been indicated in methods section

For manuscripts utilizing custom algorithms or software that are central to the research but not yet described in published literature, software must be made available to editors and reviewers. We strongly encourage code deposition in a community repository (e.g. GitHub). See the Nature Research guidelines for submitting code & software for further information.

Data

Policy information about availability of data

All manuscripts must include a data availability statement. This statement should provide the following information, where applicable:

- Accession codes, unique identifiers, or web links for publicly available datasets
- A list of figures that have associated raw data
- A description of any restrictions on data availability

Sequence data (mRNA-seq, nanoPARE-seq, sRNAseq and LTR-seq) that support the findings of this study have been deposited at the European Nucleotide Archive (ENA) under the accession code ERP118841. The mass spectrometry proteomics data have been deposited to the ProteomeXchange Consortium with the dataset identifier PXD013891.

Field-specific reporting

Please select the one below that is the best fit for your research. If you are not sure, read the appropriate sections before making your selection.

☒ Life sciences ☐ Behavioural & social sciences ☐ Ecological, evolutionary & environmental sciences

For a reference copy of the document with all sections, see nature.com/documents/nr-reporting-summary-flat.pdf

Life sciences study design

All studies must disclose on these points even when the disclosure is negative.

Sample size	Sample size was the largest possible to enable a robust statistical analysis
Data exclusions	No data was excluded from the analysis
Replication	All experiments included biological replicates. Details are indicated in figure legends
Randomization	Samples were randomly collected
Blinding	Data collection and analysis was blinded to the authors.

Reporting for specific materials, systems and methods

We require information from authors about some types of materials, experimental systems and methods used in many studies. Here, indicate whether each material, system or method listed is relevant to your study. If you are not sure if a list item applies to your research, read the appropriate section before selecting a response.

Materials & experimental systems

n/a	Involved in the study
☐	☒ Antibodies
☒	☐ Eukaryotic cell lines
☒	☐ Palaeontology and archaeology
☒	☐ Animals and other organisms
☒	☐ Human research participants
☒	☐ Clinical data
☒	☐ Dual use research of concern

Methods

n/a	Involved in the study
☒	☐ ChIP-seq
☒	☐ Flow cytometry
☒	☐ MRI-based neuroimaging

Antibodies

Antibodies used	anti-MAGO1 and anti0MAGO2 antisera were generated using a commercial supplier and immunopurified using specific peptides. Details are provided in methods section.
Validation	Antisera was validated using custom peptides and experimentally with purified proteins.